Sustainable Energy, Grids and Networks 39 (2024) 101455

Contents lists available at ScienceDirect

Sustainable Energy, Grids and Networks

journal homepage: www.elsevier.com/locate/segan

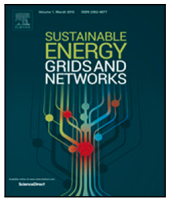

Evaluation of possible network states in the future German hydrogen network 2025 and 2030

Tobias Triesch [a], Theresa Klütz [a], Jochen Linßen [a], Detlef Stolten [a,b]

[a] Forschungszentrum Jülich GmbH, Institute of Energy and Climate Research – Techno-economic Systems Analysis (IEK-3), Wilhelm-Johnen-Straße, Jülich, 52425, Germany

[b] RWTH Aachen University, Chair for Fuel Cells, Faculty of Mechanical Engineering, Eilfschornsteinstraße 18, Aachen, 52062, Germany

ARTICLE INFO

Keywords:
Natural gas
Hydrogen
Gas network
Network development plan
Pipeline reassignment
National hydrogen strategy

ABSTRACT

This study provides insights into possible future gas network states in the initial German hydrogen network by 2025 and 2030, as per the German transmission system operators Network Development Plan Gas 2020. Not only is the overall transport feasibility assessed, but also possible operating conditions in terms of pressures, flows and velocities. To that end, two data sets for the network topology by 2025 and 2030 were created. A heuristic, semi-random nomination generation is employed to generate 100 consistent steady-state source–sink nominations for both years, based on collected production/consumption bounds. The authors employ a so-called nomination-validation model (MILP-formulation) for the solution of the resulting transport problem(s). For the evaluation of pipeline flow velocities, the authors combine those solutions with a hypothesis on limiting flow speeds suggested in a German technical journal. The analysis exhibits feasibility among all generated nominations with respect to flows and admissible velocities.

1. Introduction

The installation of a German, and ultimately pan-European, hydrogen gas network is an established plan. Politically adopted in the form of the National Hydrogen Strategy [1] in Germany and the European hydrogen strategy [2]/European Green Deal [3] in the EU, these directives reflect the importance of hydrogen for the energy transition. In fact, hydrogen technology is seen as a key component of a successful net-zero energy transition through 2045. The German gas transmission system operators (TSO(s)) have pressed ahead and conducted a survey among industrial companies in Germany, asking which of them would be interested in either consuming or producing hydrogen and in which quantities. The results of this survey have found their way into the German *Gas Network Development Plan 2020–2030* (GNDP2020)[1] [4]. Bringing together survey results and expert knowledge, the TSOs pointed out current natural gas pipelines that will be reassigned as part of a new hydrogen network that interconnects a subset of these industrial partners and future *green hydrogen* production sites. The initiative is planned to expand over the next three decades to become a pan-European hydrogen network.

The transition to hydrogen is of public interest, and yet network- and industry data is often not publicly available, is scattered over different sources or only available in insufficient detail for modeling. Therefore, this study constitutes a first effort to model the future hydrogen network (by 2025 and 2030) independently, on the basis of openly available data.

To that end, this work provides an assessment (feasibility, pressures, flows) of pseudo-random load scenarios/nominations in a model of the future German hydrogen gas network by 2025 and 2030 as stated in the GNDP 2020 and based on own project research. In addition to the feasibility aspects of individual nominations considered, an evaluation of estimated flow speeds across the set of nominations is presented. The resulting flow speeds are put into context with an equivalence hypothesis regarding the maximum allowable flow speeds given in the literature (non-research/industry journal, [5]).

The remainder of this paper is structured as follows: First, a short introduction regarding, the installation of the hydrogen network, is given. Section 2 outlines the aforementioned equivalence hypothesis, followed by the data modeling/generation for the network topology and load scenarios/nominations. Based on the initial materials and their extent, the gas network modeling literature is reviewed, and a suitable model presented. The results for the 2025 and 2030 networks are presented in Section 3. The paper is closed by a discussion (Section 4).

Background. Hydrogen is a versatile commodity that can be used as a fuel, an energy carrier or direct feedstock. Its most favorable characteristic is that it neither emits CO_2 nor other harmful compounds, when used, and can be produced in a CO_2-neutral manner (see Table 1).

E-mail address: t.kluetz@fz-juelich.de (T. Klütz).

[1] The plan is issued every two years and spans a rolling horizon of ten years.

https://doi.org/10.1016/j.segan.2024.101455
Received 22 May 2023; Received in revised form 27 February 2024; Accepted 17 June 2024
Available online 20 June 2024

Table 1
Hydrogen properties - advantages and disadvantages.

Advantages	Disadvantages
+ Can be CO_2-neutral in production and consumption	- Metals can be sensitive to hydrogen embrittlement [7]
+ Versatile (energy carrier, fuel, feedstock)	- Low volumetric energy density [8]
+ Fairly abundant in nature (in non-elemental form)	- Production needs pure water supply
+ Non-toxic to the environment [8]	- Odorless [8]
+ Established production processes exist[9]	- Relatively reactive [10]
+ Can be handled safely [10][7]	
+ Can be stored over longer periods of time	
+ High specific energy density [8]	

This makes it the ideal commodity to drive the decarbonization of several economic sectors. Although renewable electricity is expected to play the most important role in the future energy system, there are sectors, such as the chemical and process industries, that are difficult to decarbonize without hydrogen [2,6]. Hydrogen is already present and essential in the chemical industry today, but is primarily produced from fossil fuels via steam-methane-reforming (SMR)(so-called *gray hydrogen*) and accounts for 70–100 million tons of CO_2 emissions annually in the EU [2]. Thus, replacing it with renewably-generated hydrogen (so called *green hydrogen*), offers significant decarbonization potential. Furthermore, other processes, such as steel production, can be fueled by hydrogen. Currently, the direct reduction process is being tested by multiple steel manufacturers (e.g., Salzgitter AG: SALCOS [11], ThyssenKrupp Europe AG: #tkH2Steel [12] and ArcelorMittal Germany Holding GmbH [13]). However, hydrogen is not only an important commodity for the chemical and process industries, but also for other sectors and the energy system as a whole. To make the best use of renewable production capacities and transition base-load power generation to sustainable fuels over time, CO_2-neutral energy storages decoupling from energy supply and demand at different timescales, as well as the means to transport large amounts of energy efficiently over long distances, are needed. For short-term storage, batteries are an attractive option. For mid- to long-term storage, however, battery-storage systems are not currently cost-effective (compare e.g. [14,15]). Moreover, high-voltage lines exhibit significant transmission losses over large distances. A hydrogen network with storage caverns could alleviate these problems. However, establishing a new hydrogen infrastructure is no small feat and will take time. There are major challenges that must be overcome along the way, including: cost mitigation, regulation, and technical implementation. On the technical side, the prospect of "sector coupling" between natural gas, hydrogen, and electricity under volatile conditions places single- and multi-commodity network simulation within the scope of science and industry to address plannable and unplannable scenarios and ensure safe and timely energy supplies. Although the initial German hydrogen network is a purely industrial one, sooner or later it is likely to also affect the lives of the general public. Therefore, transparency and discourse on the developments under way are of importance, which is the motivation for this work.

2. Materials and methods

This chapter provides some background information on the aforementioned hypothesis regarding admissible flow speeds, and is followed by the materials and methods sections. The materials section explains the topology and data generation for the hydrogen networks, whereas the methods section justifies the choice of model for the subsequent calculations.

2.1. Flow speed hypothesis

Practical flow speed restrictions in gas pipelines are sometimes referred to as a guideline for pipeline capacity estimation and sizing. As a result, they are sometimes referenced when estimating the transport capacities of current natural gas pipelines for future hydrogen transport. It is important, however, to understand that these do not present strict technical or physical limitations. They are rather an expression of common and best practices in natural gas network operation. From an investment point of view, a smaller-diameter pipeline with higher flow speeds is favorable [16]. A high flow speed also enables high transport volumes. At the same time, higher flow speeds increase flow turbulence and, therefore, friction and pressure drop alongside noise pollution, vibrations, and operating costs associated with recompression [16]. There are also minor safety concerns involved that may apply more to older networks: Sediment particles and liquids may be picked up by the gas stream and have abrasive effects on downstream assets [16]. [5] addresses the topic of flow speed restriction and equivalent admissible flow speeds for hydrogen transport, citing scientific studies on pickup velocities for particles and liquids that discourage reasoning in favor of a flow speed restriction based on pickup velocities, as these already occur much sooner than the usual 10–20 m/s range. [5] puts forward the hypothesis that equal wall shearing stress τ_W may be the correct basis for locally equivalent stress on the pipeline, when switching from natural gas to hydrogen (see Eq. (1)).

$$\tau_W = \frac{\lambda_1(D,k,Re)}{4}\left(\frac{\rho_{NG}(p,T)}{2}v_{NG}^2\right) = \frac{\lambda_2(D,k,Re)}{4}\left(\frac{\rho_{H_2}(p,T)}{2}v_{H_2}^2\right) = \text{const.} \tag{1}$$

Here $\lambda_{\{1,2\}}(D,k,Re)$ denote the friction coefficients depending on pipeline diameter D, integral pipeline roughness k, and Reynolds number Re. ρ_i, and v_i, $i \in \{H_2, NG\}$, denote the density and velocity, respectively. Taking the limit $\lim_{Re\to\infty}\lambda(D,k,Re) = \lambda(D,k)$, results in a friction coefficient independent of the Reynolds number. Consequently, Eq. (1) can be rearranged as follows:

$$v_{H_2} = v_{NG}\sqrt{\frac{\rho_{NG}(p,T)}{\rho_{H_2}(p,T)}}. \tag{2}$$

This yields (relative) velocity ratios v_{H_2}/v_{NG} ranging from 2.87 (1 bar, 10 °C) to 3.30 (100 bar, 10 °C).[2] However, in order to obtain a direct definition of limiting stresses, [5] sets a limit on the admissible wall shearing stress $\tau_W \leq \overline{\tau}_W$. Thus, a maximum admissible velocity can be given for each gas temperature, pressure, and pipeline diameter, as per Eq. (3):

$$\overline{v} = \sqrt{\frac{\frac{8\overline{\tau}_W}{\lambda}}{\rho(p,T)}} = \frac{C}{\sqrt{\rho(p,T)}}. \tag{3}$$

For simplification, [5] suggests the use of a C-value of $125\sqrt{\text{Pa}}$ for plain steel pipes, and of $200\sqrt{\text{Pa}}$ for flow-coated ones. These C-values are averages based on estimates for the inner pipe roughness λ and wall shear stress $\overline{\tau}_W$ resulting from design velocities between 10–15 m/s and 20–25 m/s respectively. [5] points out the analogy of Eq. (3) to the so-called erosional velocity known from the literature; see, e.g., API RP14E. Own calculations show a maximum C-value for natural gas (101 bar, 283.15 K) of 93.64 $\sqrt{\text{Pa}}$ for a design velocity of 10 m/s

[2] Calculated using the CoolProp Python-Interface.

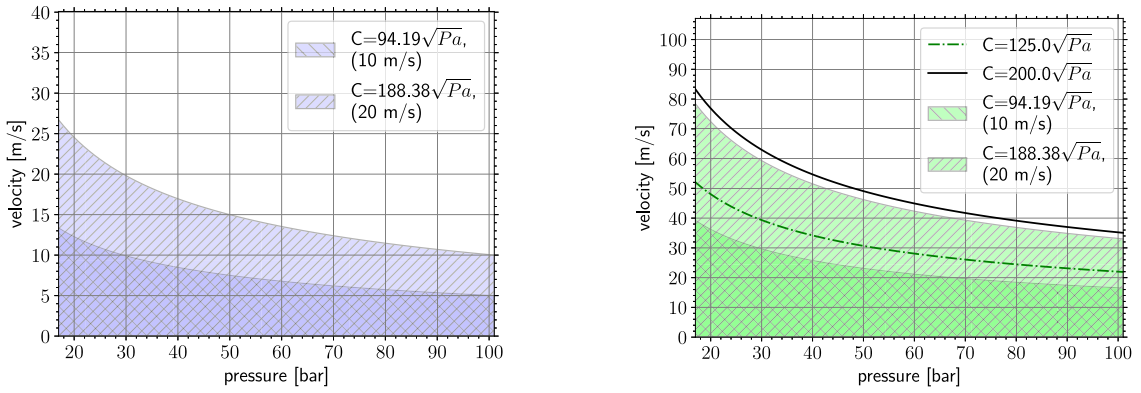

(a) natural gas (b) hydrogen

Fig. 1. Feasible pressure–velocity regions for hydrogen and natural gas for different maximum C-values, i.e., different design velocities of 10 m/s and 20 m/s, respectively. Safety factor= 2, T=283.15 K. The pressure range is 17-101 bar.

Table 2
Typical, relevant data attributes of published pipeline measures.

Attribute
– ID
– Short description
– Pipeline length
– Pipeline diameter (sometimes aggregated)
– Max. nominal pressure-level
– Map of the respective pipeline
– Estimated year of completion

and 187.28 $\sqrt{\text{Pa}}$ for a design velocity of 20 m/s. Please note that in operation flow velocities typically do not represent hard constraints.

Fig. 1 displays the resulting feasible regions for pressure–velocity tuples for natural gas (Fig. 1(a)) and hydrogen (Fig. 1(b)), based on different design velocities. The upper bounds shown include a safety factor of 2. In this work, these velocity restriction considerations, will be used to assess the simulation results for the future German hydrogen network, the modeling of which will be presented in the following section.

2.2. Materials

The modeling of real-world systems is not independent of data and more often than not that data is limited with respect to completeness, correctness and level of detail. Consequently a data-oriented approach has to be taken, followed by the modeling, which is contrary to the more common scientific approach, where precise and elaborate model development tends to precede data preparation. Therefore, an initial assessment of what data is available is essential to ensuring that the model's granularity matches the data while preserving the system's characteristic features.

For the initial German hydrogen network, the data can be divided into network (topology) and load or transport types. The former is based on hydrogen-related pipeline measures stated in the *Green gas variant* of the GNDP2020.[3] They are listed in the public transparency database of the German TSOs [17].

Table 2 presents a table of data attributes given for each pipeline measure in the transparency database that are relevant in the context of flow simulations.

[3] Note, that these studies were conducted prior to the publishing of the more recent Gas Network Development Plan 2022.

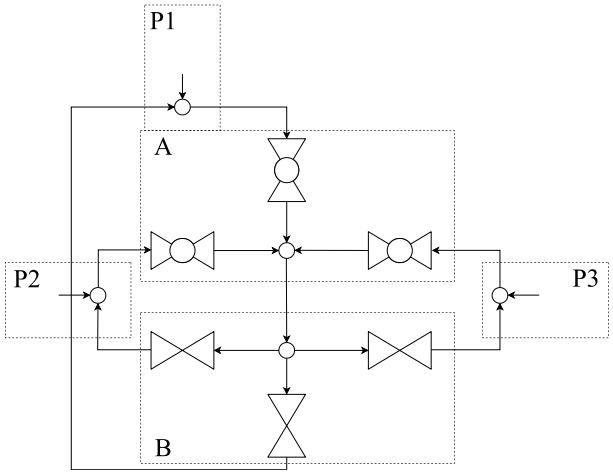

Fig. 2. Schematic view of the interconnections at junctions of the network. P1, P2, P3 denote incoming pipelines of the junction. All incoming streams can be equalized, with respect to their pressure, by means of pressure control valves (A) and leave the junction with the same pressure. The pressure control valves are complimented by shut-down valves at the outlets (B) to enable all flow directions.

The map-pictures mentioned in Table 2 were collected, geo-referenced by hand using the open-source GIS software QGIS (version 3.10) [18], and manually enriched with the presented information. No information was available on how the pipelines are interconnected. Therefore, suitable routing interconnections are put in place at junctions of the network graph (see Fig. 2).

All incoming streams can be equalized, with respect to their pressure, by means of pressure control valves and leave the junction with the same pressure. The inner pipeline roughness is assumed to be 0.1 mm, as is customary for high-pressure transmission pipelines with *small degrees of network meshing* (see [16]). The resulting network consists of pipelines, valves and pressure control valves, only. No internal network compressors or compressor stations are assumed. No statements on compressors or compressor stations to be placed in the network were reported. Which makes sense, since intermediate compression would economically speaking only be considered if there is a need for it to enable transport which would manifest in our setting in the infeasibility of transport scenarios. Such a case (not present here) would need further investigation and present the additional problem of optimal compressor station placement within the network.

Subsequently, hydrogen sinks, and sources are allocated to the network nodes, on the basis of openly-available project information.

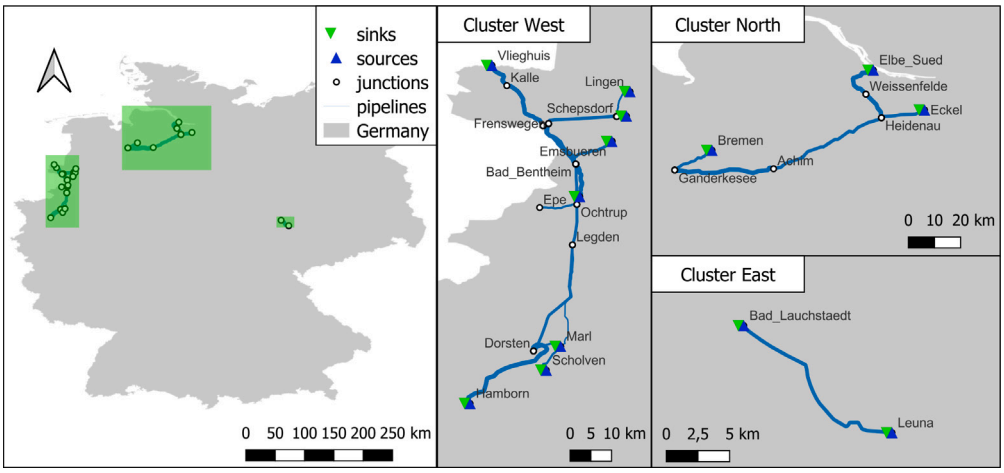

Fig. 3. Initial German hydrogen network by 2025 as per GNDP 2020. Left: Overview of the hydrogen clusters of Germany; right: close-ups of the clusters and their modeled nodes (source/sink/junction).

Initially, the authors intended to use only data from the GNDP2020; however, the level of detail of the given data is insufficient. Therefore, projects associated with the GNDP2020 market survey were surveyed for data, that could be attributed to a particular network node and added. Sources are often given in terms of the electrical power rating of a planned electrolysis site (e.g. 100 MW_{el}), some of which are directly associated with wind parks and others with proximity to the electrical grid. Here, a generic thermal efficiency of 70 percent was assumed. In some cases there are conflicting statements from different sources. In this instance, the one that results in a higher rating is selected. The collected information on potential sinks and sources can be found in Appendices B and C. The network topology can be taken from Figs. 3 and 4.

From Fig. 3, it is apparent that there exist three independent network clusters (West, North and East) marked in green on the left. Cluster West stretches from the Emsland region to the Ruhr one. Major hydrogen sources include the import point in Vlieghuis, the electrolysis site at Lingen-Hanekenfähr as well as electrolysis from wind power in Emsbüren and Ochtrup. The planned connection to the underground storage (UGS) in Epe can be observed. The sinks are primarily located in the Ruhr region, comprising the Marl chemical site, the BP Gelsenkirchen refinery (Scholven), and Thyssenkrupp Europe's steel plant in Hamborn. A further chemical site, which was assumed to act primarily as a sink in earlier years, is the chemical site at Lingen. For the 2025 network, cluster North features only a single sink/source at the Stahlwerke Bremen steel plant. Elbe Süd and Eckel could not be assigned a particular purpose in this scenario. As a result, no transport will take place in that cluster in the 2025 scenario. Cluster East comprises only a single pipeline connecting the electrolysis and storage site Energiepark Bad Lauchstädt with the Leuna chemical site.

By 2030 the clusters West and East are fully connected with notable extensions in the north-west towards Nüttermoor, Löningen and Oude-Statenzijl, in the east towards Drohne and Hallendorf as well as in the south-west towards Elten. Additionally, there are potential UGS sites in Nüttermoor and Harsefeld. Oude-Statenzijl and Elten are also import points around the Netherlands. For 2030, the GNDP assumes a switch of the import allocation from Vlieghuis to Elten without any specific explanation. At Hallendorf, Salzgitter Flachstahl steel plant is connected to the network. Further sources from wind power are located at Löningen, Drohne and Albachten. For a more detailed description, the interested reader is referred to [4].

Maximum power ratings do not readily lend themselves to scenario calculations, as they only present upper/lower bounds on the possible gas injections to, and withdrawals from, the network. In the absence of historical data, several approaches can be pursued to generate actual transport scenarios:

1. Hand-crafted single scenarios (easy to interpret, little possibility for extrapolation, author-bias)
2. Generation of potential time-series for production and demand (standard, but may be error-prone (assumptions, bias), operating regime of production facilities unknown, under given circumstances, to assess network characteristics, unnecessary).
3. Generation of random/pseudo-random load scenarios. (Focus: screening of network properties/characteristics should be relatively independent of assumptions regarding the systems' surroundings. Does not discriminate between likely and unlikely scenarios).

In the absence of precise knowledge of technical upstream and downstream specifications, as well as the initial states of the network and transients of inputs and outputs, the authors opted for the pseudo-random load scenario generation of steady-state nominations. The approach follows the idea of a regression problem. For each sink and source, there is a known upper and lower bound for network injection/withdrawal. A candidate flow for each sink and source can be drawn from a uniform distribution over its bounding interval. Although random, this collection of candidate flows is unlikely to add up to zero, which is a requirement to fulfill the steady-state flow-balance in the network. In this work we identify such a candidate nomination as noisy data, that can be entered into a regression problem to determine the closest-distance nomination that fulfills the flow-balance. The optimization framework also allows for the addition of further constraints, which comes in handy for handling sources that have a joint upper bound, instead of individual ones. The optimization problem is stated in Eqs. (4)–(15) [19].

$$\min_{\mathbf{u}} \sum_{i\in L} u_{1i}^{+} + u_{1i}^{-} + u_{2i}^{+} + u_{2i}^{-} \tag{4}$$

$$\underline{x}_i^{+} \le x_i^{+} \le \overline{x}_i^{+} \qquad \forall i \in L, \tag{5}$$

$$\underline{x}_i^{-} \le x_i^{-} \le \overline{x}_i^{-} \qquad \forall i \in L, \tag{6}$$

$$u_{1i}^{+}, u_{1i}^{-}, u_{2i}^{+}, u_{2i}^{-} \in \mathbb{R}_0^{+} \qquad \forall i \in L, \tag{7}$$

$$y_i \in \mathbb{B} \qquad \forall i \in L, \tag{8}$$

$$\sum_{i\in L} x_i^{+} + x_i^{-} = 0 \qquad , \tag{9}$$

$$\sum_{j\in C_i} x_j^{+} + x_j^{-} = 0 \qquad \forall i \in N_C, \tag{10}$$

$$u_{1i}^{+} - u_{2i}^{+} = x_i^{+} - d_i \qquad \forall i \in L, \tag{11}$$

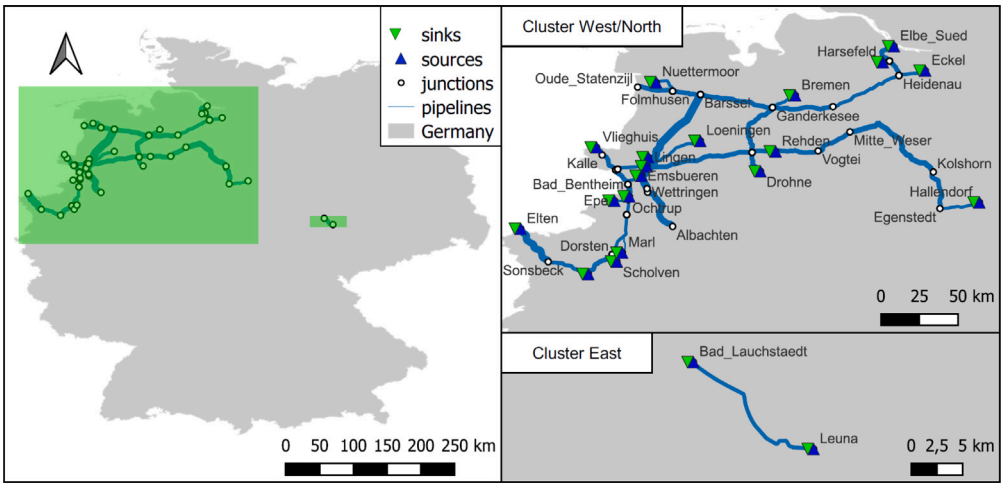

Fig. 4. Initial German hydrogen network by 2030 as per GNDP 2020. Left: Overview of the hydrogen clusters of Germany; right: close-ups of the joined clusters West/North and cluster East and their modeled nodes (source/sink/junction).

$$u_{1i}^{-} - u_{2i}^{-} = x_i^{-} - d_i \qquad \forall i \in L, \tag{12}$$

$$\sum_{j \in E_i} x_j^{+} \geq k_i \qquad \forall i \in N_E, \tag{13}$$

$$\underline{x}_i^{-} y_i \leq x_i^{-} \leq \overline{x}_i^{-} y_i \qquad \forall i \in L, \tag{14}$$

$$\underline{x}_i^{+}(1 - y_i) \leq x_i^{+} \leq \overline{x}_i^{+}(1 - y_i) \qquad \forall i \in L. \tag{15}$$

The objective represents the sum of absolute differences $|x_i^{+} - d_i|$, $|x_i^{-} - d_i|$ (right-hand side of Eqs. (11)–(12)) between to-be-determined source/sink-flows and candidate source/sink-flows. For each location, $i \in L$, a source variable x_i^{+} and sink variable x_i^{-} is introduced (Eqs. (5)–(6)), as well as a binary variable y_i (Eq. (8)), which, together with Eqs. (14)–(15), ensure mutual exclusion of simultaneous source and sink flows at a given location. Eq. (9) is the zero-sum network flow balance and Eq. (10) specifies zero-sum (sub-)flow balances over clusters $C_i, i \in N_C$ representing disconnected subnetworks. Eq. (13) specifies joint lower bounds k_i on source nodes $j \in E_i$ in node collections $i \in N_E$. This condition can be used to enforce the generation of more challenging transport scenarios in terms of the net flow within the network. The problem makes use of a $\|.\|_1$-norm formulation (Eq. (4), (7) and (11)–(12)) to minimize the distance of a candidate transport scenario, represented by $d_i, i \in L$, from a transport scenario that fulfills the additional constraints. The variables $u_{1i}^{+}, u_{1i}^{-}, u_{2i}^{+}, u_{2i}^{-}, i \in L$ are part of the $\|.\|_1$-norm formulation and represent the positive/negative parts of the absolute-value function. For the scenario analyses conducted in this work, two sets of 100 nominations are generated, one for the 2025-network and one for the 2030-network. To promote the generation of more challenging nominations, we require each nomination to exceed the limit of 50% of the maximum source–sink flow implied by the given production and consumption bounds. To establish that limit, a max-flow-problem derived from formulation (4)–(15) was solved (omitted here). The resulting source–sink-flow distributions are visualized in the form of box plots in Fig. 5 for 2025 and Fig. 6 for 2030-one.

Loads are both stated in terms of mass flow and thermal power. The bounding boxes around each quartile representation states the upper- and lower-bounds from which the candidates were drawn. From Figs. 5 and 6 it can be observed that for most sources and sinks the resulting nomination flows spread across the whole admissible range of their production/consumption range, which was the goal. At the same time it can be observed that distributions for single sources and sinks vary. In Fig. 5 Bremen exhibits no flow under no scenario as cluster North has no production or consumption facilities connected. The maximum actual import at Vlieghuis in 2025 can be seen to be implicitly limited by the maximum possible consumption of all sinks combined.

The following subsection briefly outlines the model implemented for the analyses of the networks in this study.

2.3. Methods

2.3.1. Literature review

Although no studies analyzing the hydraulic network characteristics of the anticipated future German hydrogen network are known to the authors, gas network modeling has been covered extensively in the related literature. The most common aims of gas network modeling are to assess the feasibility of transport scenarios, minimize transport costs, and plan network extensions. Mathematically, a gas network can be described as a directed graph $G = (V, E)$ that is composed of vertices/nodes $v \in V$ and edges $e \in E$. Here, vertices represent sources, sinks or junctions, whereas edges are components, such as pipelines, valves, and compressors. The usual starting point for modelers is the 1-D Euler equations in the form depicted in Eqs. (A.1)–(A.3), which describe the gas dynamics in a pipe [20–23]. The Euler equations belong to the family of hyperbolic partial differential equations (PDE(s)) and contain conservation laws for mass, momentum and energy densities. Together with suitable initial and boundary conditions, supplemented by an equation of state for the description of gas properties (Eq. (A.4)), as well as a friction model (Eq. (A.5)), they are sufficient to describe the flow of gas in a pipe. Gas network models primarily differ in the handling of the Euler equations (simplifications, model hierarchies, and discretizations) and in the handling of switchable components,[4] such as valves (mixed-integer programming (MIP)-techniques; see, e.g., [21]) or compressors (see, e.g., [24]). Fundamental theorems on partial differential equations can be found in [25]. At the same time, there exist a myriad of discretization techniques (finite difference, finite element, finite volume, spectral methods) for their computational solutions. Among these techniques finite volume approaches, based on the so-called weak formulation, appear to be the most popular [22,23], whereas spectral methods can be deemed classical. For gas network modeling, it is important to distinguish between stationary and transient flows [21,26]. Stationary network flows can be described via systems of differential algebraic equations (DAE(s)), whereas transient flows require the solution of systems of parabolic or hyperbolic partial differential equations (PDE(s)). PDEs are much more difficult to solve than DAEs containing only ordinary differential equations (ODEs) and

[4] Networks containing/lacking switchable elements are sometimes called active/passive networks.

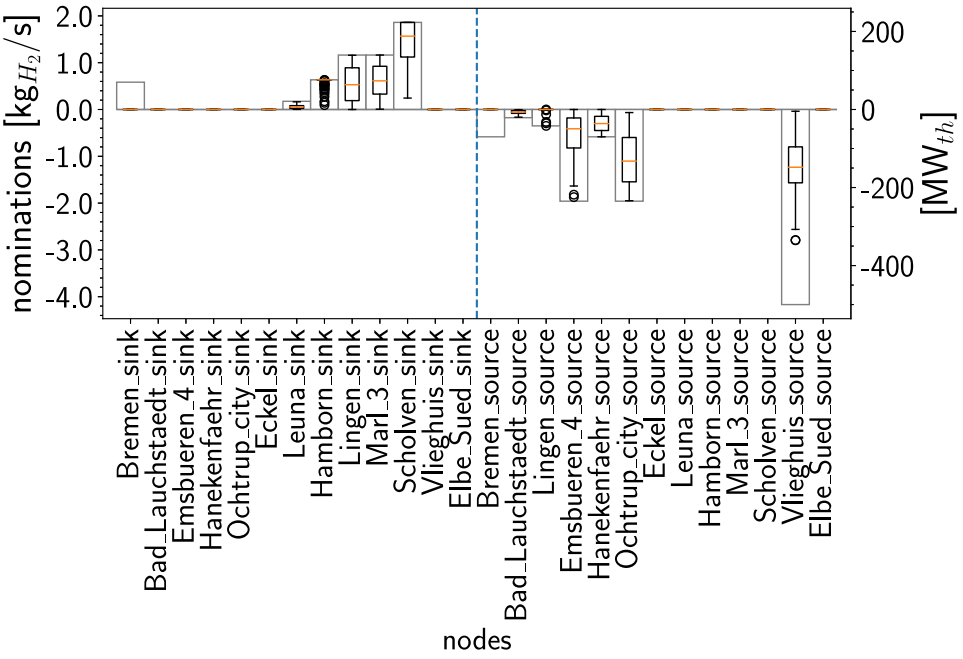

Fig. 5. Box plot source–sink-flow distribution for the 2025 network. The bounding boxes signify the original flow bounds from which candidates were drawn, whereas the quartile markers and their outliers (small circles) show the distribution of the actual source–sink-flows calculated. Every potential source- or sink-node is listed once as source (right) and once as sink (left).

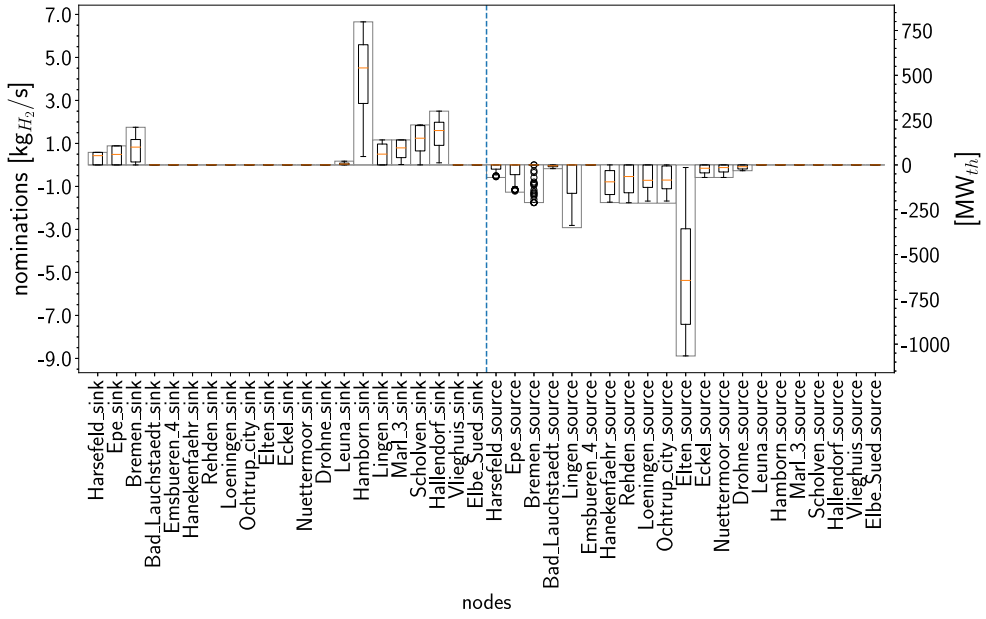

Fig. 6. Box plot source–sink-flow distribution for the 2030 network. The bounding boxes signify the original flow bounds from which candidates were drawn, whereas the quartile markers and their outliers (small circles) show the distribution of the actual source–sink-flows calculated. Every potential source- or sink-node is listed once as source (right) and once as sink (left).

algebraic equations. [21,26] explain that stationary models are best suited for cases in which the available data is not sufficient for a transient description. In particular, this can be the case for the evaluation of current and future gas network capacities, where neither the network state nor the transport scenario are known. Methods from that area are reviewed in chapter 5 of [21], and in [27,28]. [26] emphasizes that gas transport in a network should be seen as a transient process. At the same time, they consider stationary models as a tool to find suitable initial values for dynamic simulations. A complication to consider is that for larger networks the simultaneous consideration of both nonlinearities and switchable components is often not computationally feasible. Therefore, model hierarchies have been employed in numerous works, even for the stationary cases [21,22,26,29,30]. The primary aim is to solve an optimization problem that minimizes the transport cost for a given transport scenario, which is of practical relevance. [21] formulate an isothermal MINLP that is decomposed into a MILP-relaxation, related to a model in [31], and an NLP in which the switchable states are fixed to the solution values of the MILP-relaxation. [29] use a modified sequential linear programming (SLP)(described in [30]) approach that solves an MIP in each iteration

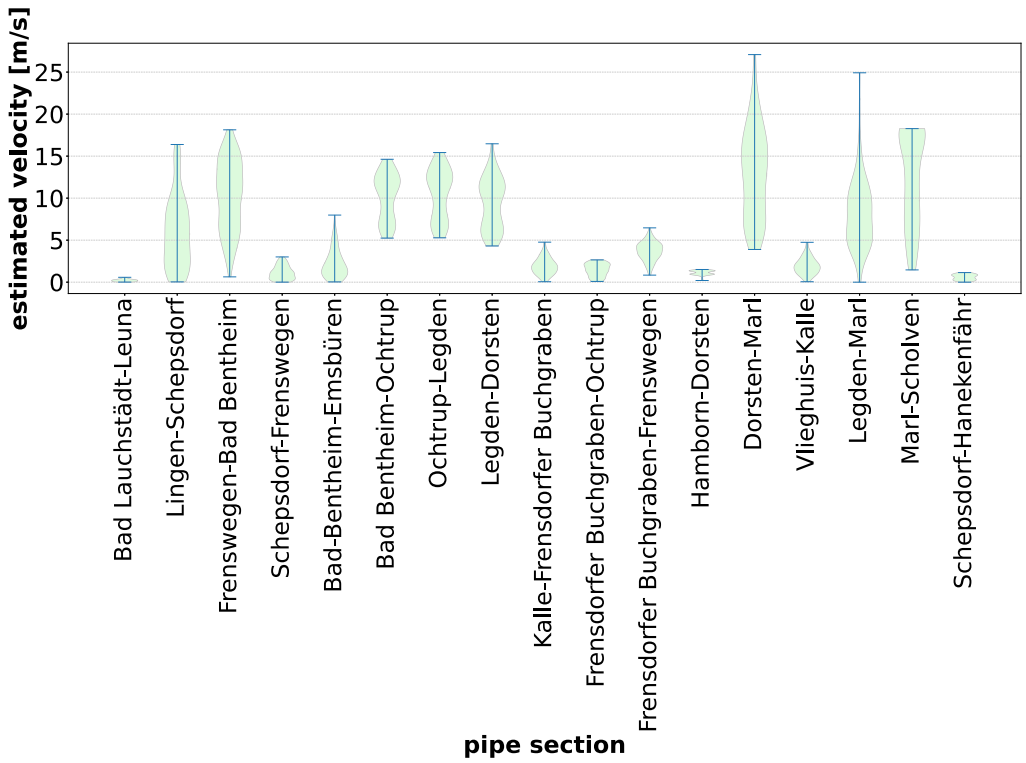

Fig. 7. Distribution of flow velocities resulting for the 2025 network.

to determine switchable states, that are fixed in the subsequent nonlinear system of equations, which is solved via Newton-like methods. The method was implemented in the commercial software GANESO [32] (Fortran 2008). The authors apply the model to the Spanish transmission network (≈ 500 nodes). [26] employ a similar approach and apply it to two networks, one being a model with 39 pipelines, 38 nodes, two compressor stations, two sinks, one valve, and the other being a model of the southern part of the National Transmission System (UK), with 95 nodes, 890 pipelines, and 32 non-pipe components. The authors of [22], on the other hand, present adaptive model hierarchies for pipe elements, for the transient and steady-state cases, as well as for isothermal and non-isothermal conditions. These can be simultaneously used in a model. They also formulate the model(s) as Port-Hamiltonian systems.[5] Direct approaches to the solution of stationary MINLPs can be found in [31,34]. The approach in [31] relies on the solution of adaptively-refined MIP-relaxations. A nomination-/transport scenario-specific bound-strengthening routine is also presented. More recently, the authors of [34] presented a decomposition approach, called a penalty-alternating direction method, to solve large-scale gas transport MINLPs with switchable components. They apply it to the real-world low- and high-calorific transmission networks of transmission system operator Open Grid Europe. In the related paper [35], the authors report on the solution of problems with more than 4000 nodes.

Conclusively, it can be said that there exists a multitude of approaches for gas network modeling and the resulting problems are challenging to solve. Stationary problems appear to remain for networks of large sizes without known system states. Optimization formulations are popular, as the main focus of network modeling is not the description of the network behavior but the optimal control thereof.

[5] On Port-Hamiltonian systems see also [33].

2.3.2. Model choice

The model employed in this study is a simplified version of chapter 6 in [21] and incorporates preprocessing methods from related work [31] as well as node-/arc-slack introduction inspired by [36]. The model is described as a mixed-integer linear program (MILP) which calculates hydraulic steady-state gas network flows under the assumption of constant average gas composition and isothermal conditions. Although, arguably more computationally intensive and less precise than a simulation model, a mixed-integer optimization formulation enables the modeler to directly consider switchable components without knowing their state a-priori. The model is applicable to large networks and requires limited information for the modeling of network components and no initial network state. This makes it well-suited for studies in the conceptual stage or where limited information is available, as is the case in this work. Within this model, a network can be composed of the following components: sinks, sources, interconnecting points, pipes, valves, automated control valves, manually-set control valves, compressors, shortcuts, linear resistors, and nonlinear resistors. The basic model is presented in the appendix. Table A.3 outlines the variable and set definitions, whereas Table A.4 defines the model parameters followed by the model Eqs. (A.6) and (A.46). Appendix A.3 explains the handling of pseudo-/squared variables. Supplementary considerations are outlined in Appendix A.4.

2.3.3. Objective function choice

The first question of interest, when dealing with potential-based flow problems is whether a certain fixed, balanced nomination can be transported by the network. This effectively makes the problem a feasibility one. That means that one is primarily concerned with finding any set of pressures, flows, and controls that satisfy all constraints. However, a suitable objective function can be used to drive the solution (if it exists) in a desirable direction. Examples would include maximizing the sum of all pressures at the nodes (establish more realistic

conditions when no precise pressure bounds are known), minimizing compression costs or investigating infeasible nominations via relaxations (introduction of artificial slack that has to be minimized). In this work, the problems were regarded as pure feasibility ones.

3. Results

The gas network model was implemented in Python 3.8, using the Pyomo optimization modeling language [37,38] and a gas properties calculation through the Coolprop-Python API [39]. 0.05 bar was chosen as the discretization tolerance for pressure variables. For flow variables, a tolerance of 0.1 kg/s was selected. A bound strengthening routine, as per [31], was used, however, without pipeline aggregation being enabled (for practical reasons). As the solver, Gurobi 9.1 [40] was employed.

For both the 2025 and the 2030 network, there exist feasible network states for all 100 nominations each. The resulting flow velocity estimations for the year 2025 are depicted in Fig. 7. The resulting pressure distribution for each network node can be taken from Fig. 8.

It can be seen that the flow velocities are mostly below even the 20 m/s limit that might be applied to natural gas networks. This shows that the flows to be transported are not challenging to the networks capabilities. The low source pressures support this indication. Pressures in the 2025 network remain within the range from 17 to 37.5 bar. At the same time, there exist pipelines that experience flow in every transport scenario, which is an indicator that these are critical to the network function and which can be verified from the network structure displayed in Fig. 3. These pipelines also exhibit great variability with respect to occurring flow speeds, as they are used in very different nominations.

The respective velocity and pressure results for the 2030 network are given in Figs. 9 and 10.

For the year 2030, flow speeds are mostly similar to the year 2025 and generally low, with few exceptions (e.g., pipeline Legden-Marl). The overall pressure level, however, does fluctuate more significantly. It should be noted that the solutions are, in general, not unique. There may even exist a set of continuous pressure ranges for which a particular nomination is feasible. Therefore, it can be taken as an effect that is due to greater degrees of freedom compared to the 2025 case.

Figs. 11(a) and 11(b) place the resulting pressure and flow velocity results in context with the equivalent shear stress hypothesis outlined in Section 2.

Fig. 11(a) shows that, for the 2025 network, all pressure–velocity pairs at the inlets/outlets of pipelines are well below the velocity bound derived from the 10 m/s design threshold of natural gas ($C=94.19\sqrt{\text{Pa}}$). In the case of the 2030 network, this holds for all pipelines, apart from Legden-Marl, which surpasses the bound into the equivalent-to-below 20-m/s stress region. Given the safety factor of two considered, it could be said that flow speeds are not critical at this stage of network operation, at least in the modeled steady-state cases.

4. Discussion

The calculations presented show that the anticipated initial German hydrogen network is not challenged by the possible loads anticipated in this study. That still holds true under consideration of flow speed restrictions derived from natural gas wall shear stress at a safety factor of two. The Legden-Marl pipeline may slightly surpass this bound in two instances, as it is a very small diameter pipeline of 200 mm. However, this is not critical on a broader scale. Depending on the future supply situation, however, awareness should be maintained that the entire connection of upper and lower network parts via Legden may exhibit bottlenecks, as it is the only connecting component between high-demand consumers and supply sources other than the Netherlands. At the same time, there are further aspects that must be addressed and considered. One aspect relates to the quality and extent

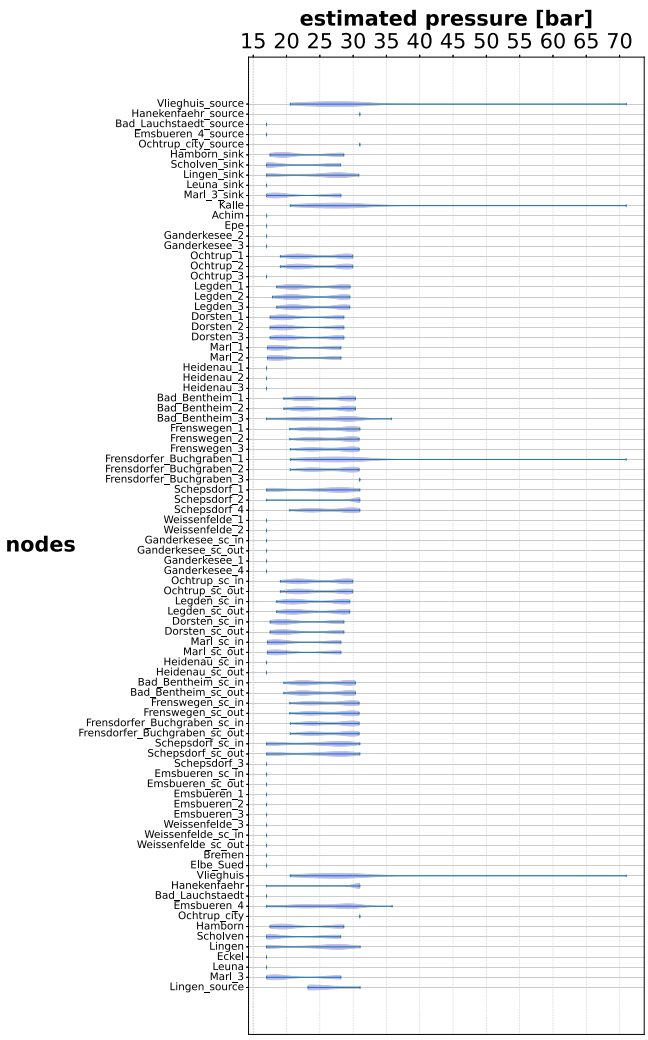

Fig. 8. Distribution of node pressures resulting for the 2025 network. On the x-axis, all network nodes are listed. The y-axis shows the distribution of absolute pressures over the 100 generated nominations.

of the available data and the assumptions made over the course of the data preparation and modeling. Data availability and quality is scarce and, therefore, error-prone. Network data rarely contains more than a pipeline (picture) and some parameters, such as length and diameter, but no switchable components, such as valves or compressors. Precise demand and production capacities are partially unknown and also corporate secrets. Therefore, it is important to acknowledge that data and mathematical modeling are not independent if data quality and resolution are not arbitrarily precise. Thus, data availability and resolution also carries over to the model selection in which the authors favored the flexibility of an optimization approach and its scalability as MILP over, arguably more precise, NLP-approaches. If more precise information becomes available, it may be more reasonable to conduct a more exhaustive study.

In the absence of such information, the authors regard the modeling of load profiles for both production and consumption as a useful tool to advance future analyses and filter out less likely load scenarios. A probabilistic analysis of the resulting load scenarios, together with network simulation/optimization, may open the door to gaining insights into the material stress caused by local pressure changes in pipes. Such load scenarios can be a starting point for analyses regarding transient network operation. Prior to that though, admissible operating conditions must be more precisely framed. The authors assumed wide admissible

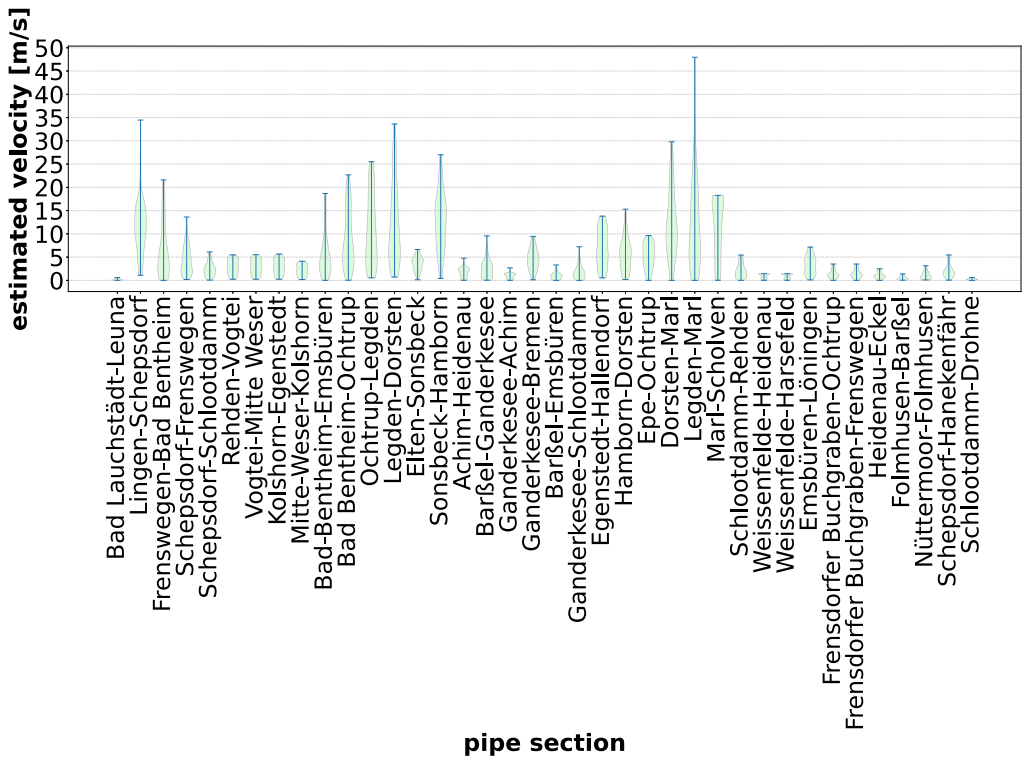

Fig. 9. Distribution of flow velocities resulting for the 2030 network.

pressure ranges that are likely to be tighter in practice, but not trivial to estimate. Given the passive nature of the network and the possibly strong fluctuations of the pressures, the minimum requirements regarding the source pressure levels to be able to control the network must be taken into account. Directly connected to that is the question of who will establish the requisite source pressure levels, i.e., the gas compression. Will it be on the production side or transportation side. Another valid question concerns what a suitable lower pressure bound for sinks, i.e., customers, would be. Naturally, these depend on customer requirements and network operating conditions. In this work, a pressure bound of 17 bar was assumed due to the fact that a lot of distribution network components are rated up to 17 bar and it may be assumed that sooner or later, distribution grids will be connected to the hydrogen network. If not required, however, pressures may be lower, which would also result in higher flow velocities throughout. Consequently, such analyses can be understood as a kind of monitoring that must be adapted over time as the network evolves and more data becomes available.

5. Conclusions

In this work we assessed the steady-state hydraulic transport feasibility of the initial hydrogen network(s) 2025/2030 as envisioned by the German network development plan 2020 and compared the resulting flow velocities to design velocities derived from a similarity approach found in the literature. For nomination generation, we presented a heuristic approach that yields balanced nominations and can consider further constraints. Our study shows the difficulties of gas network modeling of real networks based on open-source data while simultaneously showing that even with limited data, such networks can be modeled and likely future bottlenecks can be identified. Here we identified the pipeline Legden-Marl as a possible future bottleneck. The derived maximum design velocities were only exceeded in two nominations on the pipeline Legden-Marl. However, given the considered safety factor of two considered we concluded that the total network flow across the nominations is just too small to present a challenge with respect to the design velocities derived from the similarity approach.

Funding

This work was supported by the Helmholtz Association, Germany under the program “Energy System Design”.

CRediT authorship contribution statement

Tobias Triesch: Conceptualization, Data curation, Formal analysis, Investigation, Methodology, Software, Validation, Visualization, Writing – original draft. **Theresa Klütz:** Conceptualization, Methodology, Supervision, Writing – review & editing. **Jochen Linßen:** Supervision, Writing – review & editing. **Detlef Stolten:** Resources, Supervision, Writing – review & editing.

Declaration of competing interest

The authors declare that they have no known competing financial interests or personal relationships that could have appeared to influence the work reported in this paper.

Abbreviations.

The following abbreviations are used in this manuscript:

GNDP2020	Gas Network Development Plan 2020
MIP	Mixed-integer programming
NLP	Non-linear programming

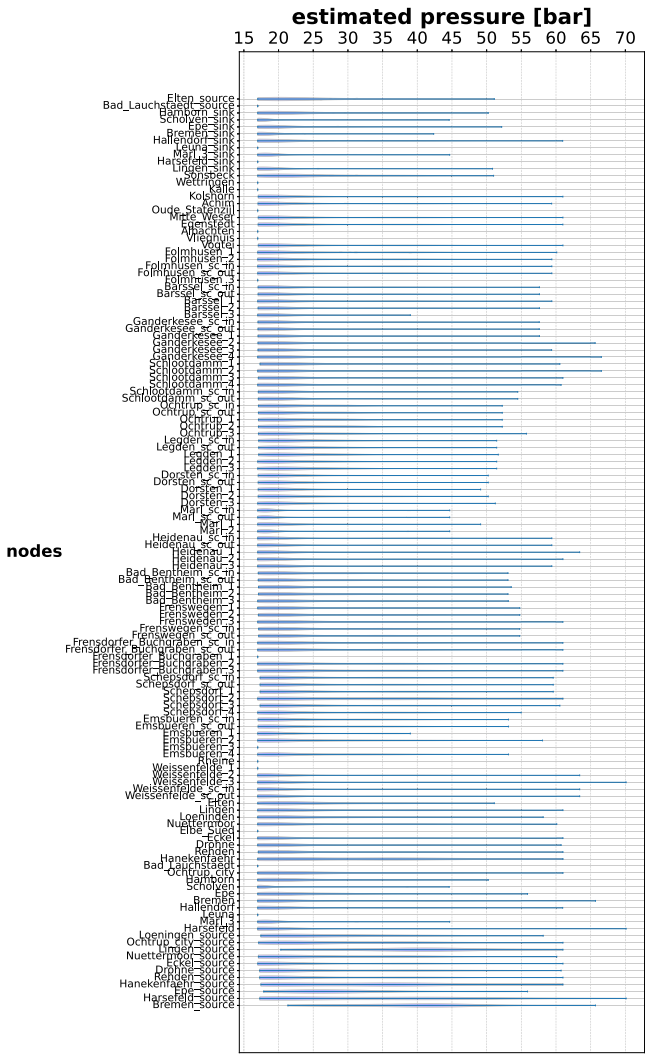

Fig. 10. Distribution of node pressures resulting for the 2030 network.

SMR	Steam-methane-reforming
TSO(s)	Transmission system operator(s)
GIS	Geographic Information System
DAE(s)	Differential algebraic equation(s)
PDE(s)	Partial differential equation(s)
ODE(s)	Ordinary differential equation(s)
SLP	Sequential linear programming
MI(N)LP	Mixed-integer (non-)linear programming
UK	United Kingdom
API	Application programming interface
Re	Reynolds number
UGS	Underground storage

Data availability

Data will be made available on request.

Appendix A

A.1.

The following 1-D Euler equations are the usual starting point for modelers of pipeline networks. The pipe model used in this paper can be derived from these equations through application of assumptions and simplifications such as steady-state and isothermal conditions as well as moderate flow velocities. The interested reader is referred to [21].

$$\frac{\partial \rho}{\partial t} + \frac{\partial (\rho v_x)}{\partial x} = 0 \qquad \text{(mass density)} \tag{A.1}$$

$$\frac{\partial (\rho v_x)}{\partial t} + \frac{\partial (\rho v_x^2)}{\partial x} + \frac{\partial p}{\partial x} = -\rho g \frac{\partial h}{\partial x} - \lambda \frac{\rho v_x^2}{2D} \qquad \text{(momentum density)} \tag{A.2}$$

$$\frac{\partial (\rho(\frac{1}{2}v_x^2 + e))}{\partial t} + \frac{\partial (\rho v_x(\frac{1}{2}v_x^2 + e) + p v_x)}{\partial x} + \frac{k_w}{D}(T - T_w) = 0 \qquad \text{(energy density)} \tag{A.3}$$

$$p = \rho R_s T z(p, T) \qquad \text{(equation of state)} \tag{A.4}$$

$$\lambda = \lambda(D, k, Re) \qquad \text{(friction model)} \tag{A.5}$$

Here ρ denotes the mass density, v_x the axial gas velocity along spatial coordinate x, p the gas pressure, g the gravitational acceleration, h the height relative to some reference height (e.g., sea-level). λ denotes the friction factor, D the pipe diameter, e the total energy, T the gas temperature and T_w the pipe wall temperature.k_w is the heat transfer coefficient, R_s the specific gas constant and z the compressibility factor. The friction model is a function of the diameter D, integral pipe roughness k, and the Reynolds number Re.

A.2. Basic gas network model (see also Chapter 6 in [21,31])

A.2.1. Sets, variables, parameters

A.2.2. Network

$$\underline{q}_a \le q_a \le \overline{q}_a \quad \forall a \in A, \tag{A.6}$$

$$\underline{p}_i \le p_i \le \overline{p}_i \quad \forall i \in V, \tag{A.7}$$

$$\sum_{k:(j,k)\in A} q_{j,k} - \sum_{i:(i,j)\in A} q_{i,j} = d_j \quad \forall i \in V. \tag{A.8}$$

A.2.3. Pipelines

$$p_i^2 - \alpha_a p_j^2 = \beta_a |q_a| q_a \quad \forall a = (i,j) \in A_{pi}, \tag{A.9}$$

$$\alpha_a = e^{-S_a} \tag{A.10}$$

$$S_a = 2\, g \frac{s_{l,a} L_a}{R_s z_m T_m} \tag{A.11}$$

$$z_m = z(p_{m,a}, T_m) \tag{A.12}$$

$$\beta_a = \begin{cases} -\frac{L_a \lambda_a R_s z_m T_m}{A_a^2 D_a} \frac{e^{S_a}-1}{S_a e^{S_a}} & \text{if slope } s_{l,a} \neq 0 \\ -\frac{L_a \lambda_a R_s z_m T_m}{A_a^2 D_a} & \text{else.} \end{cases} \tag{A.13}$$

$$\lambda_a = \frac{1}{(2log_{10}\frac{D_a}{k_a} + 1.138)^2} \tag{A.14}$$

See Nikuradse's formula [41].

A.2.4. Valves

$$\underline{q}_a s_a \le q_a \le \overline{q}_a s_a \quad \forall a = (i,j) \in A_{va}, \tag{A.15}$$

$$(\overline{p_j} - \underline{p_i}) s_a + p_j - p_i \le \overline{p_j} - \underline{p_i} \quad \forall a = (i,j) \in A_{va}, \tag{A.16}$$

$$(\overline{p_i} - \underline{p_j}) s_a + p_i - p_j \le \overline{p_i} - \underline{p_j} \quad \forall a = (i,j) \in A_{va}. \tag{A.17}$$

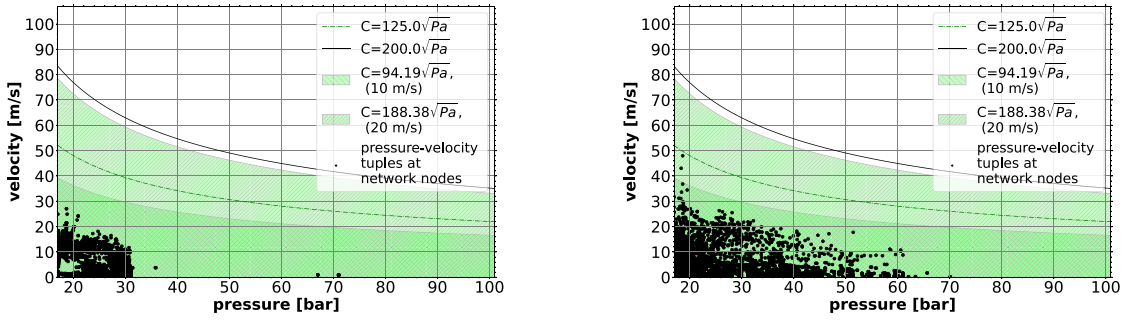

(a) 2025 (b) 2030

Fig. 11. Resulting pressure–velocity tuples for the 2025 and 2030 network nominations in the context of the velocity restriction considerations presented in Section 2.1. The C-values represent different design velocities of 10 m/s and 20 m/s, respectively. Safety factor= 2, T=283.15 K. The pressure range is 17-101 bar.

Table A.3
Sets and variables.

Set	Definition	Variable	Definition
A	Edges/arcs of the network graph	q_a	Mass flow over arc a
V	Nodes/vertices of the network graph	p_i	Pressure at node i
$A_{pi} \subset A$	Arcs that are pipelines	$s_a \in \mathbb{B}$	Integer control variable of arc a
$A_{va} \subset A$	Arcs that are valves	$r_a \in \mathbb{B}$	Flow direction indicator variable of arc a
$A_{cv}^{aut} \subset A$	Arcs that are automated control valves	$s_a^{ac} \in \mathbb{B}$	Active-mode indicator variable
$A_{cv}^{man} \subset A$	Arcs that are manually-set valves		
$A_{cs} \subset A$	Arcs that are compressors		
$A_{sc} \subset A$	Arcs that are short-cuts		
A_{rs}^{lin}	Arcs that are linear resistors		
A_{rs}^{nl}	Arcs that are nonlinear resistors		

Table A.4
Parameters.

Parameter	Definition	Parameter	Definition
$[\underline{q}_a, \overline{q}_a] \subset \mathbb{R}$	Mass flow bounds of arc a		
$[\underline{p}_i, \overline{p}_i] \subset \mathbb{R}^+$	Pressure bounds of node i		
$d_i \in \mathbb{R}$	Source/sink flow at node i		
α_a	Coefficient for potential pressure difference	D_a	Pipeline diameter
g	Gravitational acceleration	$s_{l,a} \in [-1, 1]$	Pipe slope
L_a	pipe length	R_s	Specific gas constant
z_m	Average compressibility factor	$p_{m,a}$	Average pipe pressure based on bounds
T_m	Average gas temperature in the network	β_a	Friction and gas property coefficient
λ_a	Friction coefficient	A_a	Cross-sectional pipe area
k_a	Integral pipe roughness	$[\overline{\Delta}_a, \underline{\Delta}_a] \subset \mathbb{R}^+$	Min./max. pressure reduction
p_a^{set}		$[\underline{\Delta p}_a, \overline{\Delta p}_a] \subset \mathbb{R}^+$	Min./max. pressure increase
$[\underline{\epsilon}_a, \overline{\epsilon}_a] \subset [1, \infty)$	Min./max. compression ratio	$\overline{\xi}_a$	Fixed pressure drop
ϵ	Small domain parameter for jump condition	ζ_a	Drag factor of flow-dependent resistor

A.2.5. Automated control valves

$$\underline{q}_a s_a \le q_a \le \overline{q}_a s_a \qquad \forall a = (i,j) \in A_{cv}^{aut}, \tag{A.18}$$

$$(\overline{p}_j - \underline{p}_i + \underline{\Delta}_a)s_a + p_j - p_i \le \overline{p}_j - \underline{p}_i \quad \forall a = (i,j) \in A_{cv}^{aut}, \tag{A.19}$$

$$(\overline{p}_i - \underline{p}_j - \overline{\Delta}_a)s_a + p_i - p_j \le \overline{p}_i - \underline{p}_j \quad \forall a = (i,j) \in A_{cv}^{aut}, \tag{A.20}$$

$$q_a \ge 0 \qquad \forall a = (i,j) \in A_{cv}^{aut}. \tag{A.21}$$

A.2.6. Manually-set control valves

$$s_a^{ac} + s_a^{bp} = s_a \qquad \forall a = (i,j) \in A_{cv}^{man}, \tag{A.22}$$

$$p_i - p_j \le (1 - s_a^{bp})(\overline{p}_i - \underline{p}_j) \quad \forall a = (i,j) \in A_{cv}^{man}, \tag{A.23}$$

$$p_i - p_j \ge (1 - s_a^{bp})(\underline{p}_i - \overline{p}_j) \quad \forall a = (i,j) \in A_{cv}^{man}, \tag{A.24}$$

$$p_j + s_a^{bp}(\overline{p}_j - p_a^{set}) \le \overline{p}_j \qquad \forall a = (i,j) \in A_{cv}^{man}, \tag{A.25}$$

$$p_j + s_a^{ac}(\overline{p}_j - p_a^{set}) \le \overline{p}_j \qquad \forall a = (i,j) \in A_{cv}^{man}, \tag{A.26}$$

$$p_j + s_a^{ac}(\underline{p}_j - p_a^{set}) \ge \underline{p}_j \qquad \forall a = (i,j) \in A_{cv}^{man}, \tag{A.27}$$

$$p_i - p_j \ge (1 - s_a^{ac})(\underline{p}_i - \overline{p}_j) \quad \forall a = (i,j) \in A_{cv}^{man}, \tag{A.28}$$

$$q_a \ge (1 - s_a^{ac})\underline{q}_a \qquad \forall a = (i,j) \in A_{cv}^{man}, \tag{A.29}$$

$$p_j + (p_a^{set} - \underline{p}_j) \ge p_a^{set} \qquad \forall a = (i,j) \in A_{cv}^{man}, \tag{A.30}$$

$$\underline{q}_a s_a \le q_a \le \overline{q}_a s_a \qquad \forall a = (i,j) \in A_{cv}^{man}. \tag{A.31}$$

A.2.7. Compressors

$$\underline{q}_a s_a \le q_a \le \overline{q}_a s_a \qquad \forall a = (i,j) \in A_{cs}. \tag{A.32}$$

$$p_j - p_i \ge \underline{\Delta p}_a s_a + (\underline{p}_j - \overline{p}_i)(1 - s_a) \quad \forall a = (i,j) \in A_{cs}. \tag{A.33}$$

$$p_j - p_i \le \overline{\Delta p}_a s_a + (\overline{p}_j - \underline{p}_i)(1 - s_a) \quad \forall a = (i,j) \in A_{cs}. \tag{A.34}$$

$$p_j \ge \underline{\epsilon}_a p_i - (1 - s_a)(\underline{\epsilon}_a \overline{p}_i + \underline{p}_j) \qquad \forall a = (i,j) \in A_{cs}. \tag{A.35}$$

$$p_j \le \overline{\epsilon}_a p_i - (1 - s_a)(\overline{\epsilon}_a \underline{p}_i - \overline{p}_j) \qquad \forall a = (i,j) \in A_{cs}, \tag{A.36}$$

$$q_a \ge 0 \qquad \forall a = (i,j) \in A_{cs}. \tag{A.37}$$

Table B.5
2025: Cluster East.

Node	Info	Production (capacity)	Consumption (capacity)	Entry [MWth]	Exit [MWth]	Ref.
Bad Lauchstädt (source/storage)	Energiepark Bad Lauchstädt: electrolysis, cavern storage	30 MWel		22.5	0	[4,17,42]
Leuna (sink)	Leuna chemical site		all from Bad Lauchstädt	0	22.5	[4,17]

Table B.6
2025: Cluster North.

Node	Info	Production (capacity)	Consumption (capacity)	Entry [MWth]	Exit [MWth]	Ref.
Elbe Süd (import)	unclear: maybe later connection to Brunsbüttel and Denmark and/or shipping	2030: 100 MWel electrolysis; shipping?	0	0	0	[17]
Heidenau		0	0	0	0	[17]
Achim	natural gas compressor station	0	0	0	0	[17]
Eckel (sink/source/import)	unclear what is connected here Assumption: 2030: Moorburg power station; also suitable for shipping	0	0	0	0	[17,43]
Ganderkesee		0	0	0	0	[17]
Bremen (sink/source)	Stahlwerke Bremen	2025: 100 MWel	2025: 100 MWel	75	75	[17,44]

A.2.8. Shortcuts

$$p_i = p_j \forall a = (i,j) \in A_{sc}. \tag{A.38}$$

A.2.9. Fixed pressure-drop resistors

$$\underline{q}_a r_a \le q_a \le \overline{q}_a (1 - r_a) \ \forall a = (i,j) \in A_{rs}^{lin}, \tag{A.39}$$

$$p_i - p_j = \begin{cases} -\xi_a & , q_a \le -\epsilon \\ \frac{\xi_a}{\epsilon} & , -\epsilon \le q_a \le \epsilon \\ \xi_a & , q_a \ge \epsilon. \end{cases} \quad \forall a = (i,j) \in A_{rs}^{lin}. \tag{A.40}$$

A.2.10. Flow-dependent resistors

$$\underline{q}_a r_a \le q_a \le \overline{q}_a (1 - r_a) \qquad \forall a = (i,j) \in A_{rs}^{nl}, \tag{A.41}$$

$$p_i^2 - p_j^2 + |\Delta_a| \Delta_a = 2 c_a |q_a| q_a \qquad \forall a = (i,j) \in A_{rs}^{nl}, \tag{A.42}$$

$$c_a = 8 \zeta_a R_s T_m z_{m,a} / \pi^2 D_a^4 \qquad , \tag{A.43}$$

$$\Delta_a = p_i - p_j \qquad \forall a = (i,j) \in A_{rs}^{nl}, \tag{A.44}$$

$$p_i - p_j \le (\overline{p}_i - \underline{p}_j)(1 - r_a) \qquad \forall a = (i,j) \in A_{rs}^{nl}, \tag{A.45}$$

$$p_j - p_i \le (\overline{p}_j - \underline{p}_i) r_a \qquad \forall a = (i,j) \in A_{rs}^{nl}. \tag{A.46}$$

A.3. Handling of (pseudo-) quadratic variables

The Extended Incremental Method (EIM) [31].

$$x = \hat{x}_0 + \sum_{i=1}^{k} (\hat{x}_i - \hat{x}_{i-1}) \delta_i \tag{A.47}$$

$$y = f(\hat{x}_0) + \sum_{i=1}^{k} (f(\hat{x}_i) - f(\hat{x}_{i-1})) \delta_i + e \tag{A.48}$$

$$e \le e_u^1 + \sum_{i=1}^{k-1} z_i (e_u^{i+1} - e_u^i) \tag{A.49}$$

$$e \ge -e_o^1 - \sum_{i=1}^{k-1} z_i (e_o^{i+1} - e_o^i) \tag{A.50}$$

$$\delta_{i+1} \le z_i \qquad \forall i \in \{1,2,\dots,k-1\} \tag{A.51}$$

$$z_i \le \delta_i \qquad \forall i \in \{1,2,\dots,k-1\} \tag{A.52}$$

$$z_i \in \{0,1\} \qquad \forall i \in \{1,2,\dots,k-1\} \tag{A.53}$$

$$\delta_1 \le 1 \tag{A.54}$$

$$\delta_k \ge 0. \tag{A.55}$$

Auxiliary problem for the reduction of discretization variables [21]:

$$\min \quad \sum_{i \in V} \left\lceil \frac{\overline{p}_i - \underline{p}_i}{2\sqrt{\tau}} \right\rceil (\alpha_i^p + \alpha_i^\pi) \tag{A.56}$$

subject to: (A.57)

$$\alpha_i^p + \alpha_j^\pi \ge 1 \quad \forall (i,j) \in A \setminus (A_p \cup A_\pi) \tag{A.58}$$

$$\alpha_i^\pi + \alpha_j^p \ge 1 \quad \forall (i,j) \in A \setminus (A_p \cup A_\pi) \tag{A.59}$$

$$\alpha_i^p + \alpha_j^\pi \ge 1 \quad \forall i \in V \tag{A.60}$$

$$\alpha_i^p = \alpha_j^p = 1 \quad \forall (i,j) \in A_p \tag{A.61}$$

$$\alpha_i^\pi = \alpha_j^\pi = 1 \quad \forall (i,j) \in A_\pi \tag{A.62}$$

$$\alpha_i^p, \alpha_i^\pi \in \{0,1\} \quad \forall i \in V. \tag{A.63}$$

For every node $i \in V$ two indicator variables α_i^p, α_i^π are introduced that indicate whether node i needs a pressure variable, a squared pressure variable, or both. For a discretization tolerance τ, the expression $\left\lceil \frac{\overline{p}_i - \underline{p}_i}{2\sqrt{\tau}} \right\rceil$ returns the number of discretization variables needed (in the EIM) to approximate the quadratic pressure function up to precision τ on each segment of an equidistant grid over $[\underline{p}_i, \overline{p}_i]$.

Table B.7
2025: Cluster West.

Node	Info	Production (capacity)	Consumption (capacity)	Entry [MWth]	Exit [MWth]	Ref.
Lingen (sink/source)	bp Lingen electrolysis project with Ørsted	2025:60 MWel/ 1 tonne/h (1/5 of current local SMR production) 2025+: 150 MWel 2030+: 500+ MWel	2025: 50000 N m^3/h 2030: 500+ MWel ?	45	139.5338	[45,46]
Schepsdorf		0	0	0	0	[17]
Frenswegen		0	0	0	0	[17]
Bad Bentheim		0	0	0	0	[17]
Emsbüren (source)		2025: wind onshore shared with Ochtrup 235 MWth 2030: no more?	0	235*	0	[4,17]
Ochtrup		0	0	0	0	[17]
Legden		0	0	0	0	[17]
Dorsten		0	0	0	0	[17]
Hamborn (sink)	ThyssenKrupp Steel Europe AG	STEAG will likely provide hydrogen directly locally	total demand for switch to H2: 700000 t/a 30% switch by 2030 → 2025: 20000 t/a → 2030: 210000 t/a	0	76.07	[12,17], [47]
Frensdorfer-Buchgraben		0	0	0	0	[17]
Ochtrup (city) (source)		2025: wind onshore shared with Emsbüren 235 MWth 2030: shared with Löningen and Rehden 305 MWth	0	235*	0	[4,17]
Epe (storage)	E.on Gas Storage GmbH not operational by 2025	0	0	0	0	[4,17]
Marl (sink)	Marl chemical site	SMR backup from current production available	2025: 50000 N m^3/h	0	139.5338	[17,45]
Vlieghuis (import)	import capacity assumed in GNDP 2020	500 MWth	0	500	0	[4]
Scholven (sink)	bp Gelsenkirchen	SMR backup from current production available	2025: 80000 N m^3/h	0	223.25	[45]
Hanekenfähr (source)	RWE Lingen power plant site	2025: 100 MWel supposed to supply 22000 N m^3/h continuously in the beginning 2030: ?	supposed to have a 60 MW gas turbine to produce electricity from hydrogen	75	0	[46,48], [45,49]

Table B.8
Pipeline data for the 2025-network. For the integral pipeline roughness a value of 0.1 mm is assumed everywhere.

ID	Length [km]	Diameter [mm]
Bad Lauchstädt-Leuna	20.00	500
Lingen-Schepsdorf	11.30	250
Frenswegen-Bad Bentheim	18.00	350
Schepsdorf-Frenswegen	18.00	450
Bad-Bentheim-Emsbüren	15.00	400
Bad Bentheim-Ochtrup	15.30	400
Ochtrup-Legden	15.70	400
Legden-Dorsten	38.00	400
Kalle-Frensdorfer Buchgraben	18.90	600
Frensdorfer Buchgraben-Ochtrup	29.90	600
Elbe Süd-Weissenfelde	22.10	600
Achim-Heidenau	54.20	450
Heidenau-Eckel	19.20	450
Ganderkesee-Achim	40.80	600
Ganderkesee-Bremen	17.10	400
Frensdorfer Buchgraben-Frenswegen	1.40	600
Hamborn-Dorsten	37.00	600
Epe-Ochtrup	10.00	300
Dorsten-Marl	8.00	300
Vlieghuis-Kalle	6.70	600
Legden-Marl	40.40	200
Marl-Scholven	14.00	300
Schepsdorf-Hanekenfähr	2.30	500
Weissenfelde-Heidenau	19.00	600

A.4. Additional constraints and methods

Although the basic component models describe the component characteristics of the gas network, there are both modeling and computational factors to be taken into account. On the one hand, there exist subnetworks of basic components, such as compressor stations or control valve stations, that induce a particular coupling of components that should be laid out explicitly to reduce MIP-complexity. On the other, the discretization of squared variables introduces integer variables as well, depending on the size of the interval to be discretized. Thus, it is straight forward to apply a nomination-, i.e., load-based bound-strengthening routine. The interested reader is referred to [31], as these examples are somewhat lengthy. At the same time, bound-strengthening methods are essential to making larger problems tractable.

Appendix B. 2025-network sinks/sources

See Tables B.5–B.8.

Appendix C. 2030-network sinks/sources

See Tables C.9–C.12.

Table C.9
2030: Cluster West/North (1/3).

Node	Info	Production (capacity)	Consumption (capacity)	Entry [MWth]	Exit [MWth]	Ref.
Lingen (sink/source)	bp Lingen electrolysis with Ørsted	2030: 500 MWel	2030: 50000 N m^3/h same as 2025	375	139.5338	[45,46]
Schepsdorf		0	0	0	0	[17]
Frenswegen		0	0	0	0	[17]
Bad Bentheim		0	0	0	0	[17]
Schlootdamm		0	0	0	0	[17]
Rehden (source)	wind onshore shared with Löningen and Ochtrup 305 MWth	305*	0	305*	0	[4,17]
Vogtei		0	0	0	0	[17]
Mitte Weser		0	0	0	0	[17]
Kolshorn		0	0	0	0	[17]
Egenstedt		0	0	0	0	[17]
Emsbüren (source)		2025: wind onshore shared with Ochtrup 235 MWth 2030: no more?	0	0	0	[4,17]
Löningen (source)		wind onshore shared with Rheden and Ochtrup 305 MWth	0	305*	0	[4]
Ochtrup		0	0	0	0	[17]
Legden		0	0	0	0	[17]
Dorsten		0	0	0	0	[17]
Rheine		0	0	0	0	[17]
Wettringen		0	0	0	0	[17]
Elten (import)	import capacity assumed in GNDP2020	GNDP2020: 1066 MWth	0	1066	0	[4,17]
Sonsbeck		0	0	0	0	[17]
Hamborn (sink)	ThyssenKrupp Steel Europe AG	STEAG will likely provide hydrogen locally	total demand for switch to hydrogen: 700000 t/a 30% by 2030 → 2025: 20000 t/a 2030: 210000 t/a	0	798.2	[12,17,47]

Table C.10
2030: Cluster West/North (2/3).

Node	Info	Production (capacity)	Consumption (capacity)	Entry [MWth]	Exit [MWth]	Ref.
Kalle (storage)	natural gas storage facility	0	0	0	0	[17]
Frensdorfer-Buchgraben		0	0	0	0	[17]
Ochtrup (city) (source)		2030: wind onshore shared with Löningen and Rheden 305 MWth	0	305*	0	[4,17]
Elbe Süd (import)	unclear: later connection Brunsbüttel and Denmark and shipping?	0	0	0	0	[17]
Heidenau		0	0	0	0	[17]
Achim	natural gas compressor station	0	0	0	0	[17]
Eckel (sink/source/import)	unclear what is connected here Assumption: 2030: Moorburg power station; also suitable for shipping	2030: 100 MWel electrolysis	0	75	0	[17,43]
Oude-Statenzijl	unclear: most likely future import	0	0	0	0	[17]
Folmhusen		0	0	0	0	[17]
Barßel		0	0	0	0	[17]
Ganderkesee		0	0	0	0	[17]

(*continued on next page*)

Table C.10 (*continued*).

Bremen (sink/source)	Stahlwerke Bremen	2030: 300 MWel	2030: 300 MWel	225	225	[17,44]
Nüttermoor (source)		2030: 100 MWel	0	75	0	[17]
Hallendorf (sink)	Salzgitter Flachstahl GmbH	0 0 0	3.9 mil tons of steel per year, assumption: 30% via hydrogen route: 300 MWth	0	300	[11,17]
Epe (storage)	E.on Gas Storage GmbH	152 MWth	152 MWth	152	152	[4,17]
Marl (sink)	Marl chemical site	SMR backup from current production available 2025: 50000 N m^3/h, 2030: same?	0	139.5338	0	[17,45]

Table C.11
2030: Cluster West/North (3/3).

Node	Info	Production (capacity)	Consumption (capacity)	Entry [MWth]	Exit [MWth]	Ref.
Vlieghuis (import)	import capacity assumed for 2025 in GNDP2020, but none for 2030	0	0	0	0	[4,17]
Scholven (sink)	Ruhr Öl Raffinerie Scholven /bp Gelsenkirchen	SMR backup from current production available	2025: 80000 N m^3/h assumption: 2030: same	0	223.25	[45]
Hanekenfähr (source)	RWE Lingen power plant site	2030: 300 MWel assumed	supposed to have a 60 MW gas turbine to produce electricity from hydrogen	225	0	[45,46,48,49]
Drohne (source)	unclear: BASF Polyurethanes close by future wind park Brockumer Fladder more likely; eff. 46 MWel	46 MWel	0	34.5	0	[17,50]
Harsefeld (storage)	natural gas storage: Storengy Deutschland Betrieb GmbH	2030+: 100 MWel?	100 MWel	75	75	[51]
Albachten	unclear: municipalities Steinfurt/Münster + münsterNETZ?	0	0	0	0	[17]

Table C.12
Pipeline data for the 2030-network. For the integral pipeline roughness a value of 0.1 mm is assumed everywhere.

ID	Length [km]	Diameter [mm]
Bad Lauchstädt-Leuna	20.00	500
Lingen-Schepsdorf	11.30	250
Frenswegen-Bad Bentheim	18.00	350
Schepsdorf-Frenswegen	18.00	450
Schepsdorf-Schlootdamm	72.90	600
Rehden-Vogtei	28.90	600
Vogtei-Mitte Weser	29.00	600
Kolshorn-Egenstedt	38.50	600
Mitte-Weser-Kolshorn	92.90	700
Emsbüren-Löningen	55.00	400
Bad-Bentheim-Emsbüren	15.00	400
Bad Bentheim-Ochtrup	15.30	400
Ochtrup-Legden	15.70	400
Legden-Dorsten	38.00	400
Rheine-Wettringen	3.50	800
Wettringen-Albachten	43.20	800
Elten-Sonsbeck	42.30	900
Sonsbeck-Hamborn	34.00	500
Kalle-Frensdorfer Buchgraben	18.90	600
Frensdorfer Buchgraben-Ochtrup	29.90	600
Elbe Süd-Weissenfelde	22.10	600
Achim-Heidenau	54.20	450
Heidenau-Eckel	19.20	450
Oude Statenzijl-Folmhusen	22.50	600
Barßel-Ganderkesee	47.70	600
Folmhusen-Barßel	19.20	600
Ganderkesee-Achim	40.80	600
Ganderkesee-Bremen	17.10	400
Nüttermoor-Folmhusen	18.40	400

Table C.12 (*continued*).

ID	Length [km]	Diameter [mm]
Barßel-Emsbüren	94.70	1000
Emsbüren-Rheine	13.80	1000
Ganderkesee-Schlootdamm	58.90	600
Frensdorfer Buchgraben-Frenswegen	1.40	600
Egenstedt-Hallendorf	30.00	400
Hamborn-Dorsten	37.00	600
Epe-Ochtrup	10.00	300
Dorsten-Marl	8.00	300
Vlieghuis-Kalle	6.70	600
Legden-Marl	40.40	200
Marl-Scholven	14.00	300
Schepsdorf-Hanekenfähr	2.30	500
Schlootdamm-Rehden	15.70	600
Schlootdamm-Drohne	21.50	600
Weissenfelde-Heidenau	19.00	600
Weissenfelde-Harsefeld	4.50	600

References

[1] Federal Ministry for Economics Affairs and Energy, The National Hydrogen Strategy, 2020, Federal Ministry for Economic Affairs and Climate Action, URL https://www.bmwi.de/Redaktion/EN/Publikationen/Energie/the-national-hydrogen-strategy.html.

[2] Communication from the commission to the European parliament, the council, the European economic and social committee and the committee of the regions a hydrogen strategy for a climate-neutral Europe, 2020, URL https://eur-lex.europa.eu/legal-content/EN/TXT/?uri=CELEX:52020DC0301.

[3] Communication from the commission to the European parliament, the european council, the council, the European economic and social committee and the committee of the regions the European green deal, 2019, URL https://eur-lex.europa.eu/legal-content/EN/TXT/?qid=1583420149564&uri=CELEX:52019DC0640.

[4] FNB Gas e.V., Netzentwicklungsplan Gas 2020–2030, 2020, URL https://fnb-gas.de/netzentwicklungspl%C3%A4ne/netzentwicklungsplan-2020/.

[5] J. Mischner, Zur Frage der strömungsgeschwindigkeiten in Gasleitungen, 2021, p. 20, gwf Gas Energie.

[6] D. Stolten, P. Markewitz, T. Schöb, F. Kullmann, Neue Ziele auf alten Wegen? Strategien für eine treibhausgasneutrale Energieversorgung bis zum Jahr 2045, in: Energie & Umwelt/Energy & Environment, vol. 577, Forschungszentrum Jülich GmbH, Zentralbibliothek, Verlag, 2022, URL http://hdl.handle.net/2128/31477.

[7] O.J.C. Huising, A.H.M. Krom, H2 in an Existing Natural Gas Pipeline, in: Volume 1: Pipeline and Facilities Integrity, American Society of Mechanical Engineers, Virtual, Online, 2020, V001T03A057, http://dx.doi.org/10.1115/IPC2020-9205, URL https://asmedigitalcollection.asme.org/IPC/proceedings/IPC2020/84447/Virtual,%20Online/1095967.

[8] Rechnen Sie mit Wasserstoff. Die Datentabelle, 2013, URL https://www.linde-gas.at/de/images/1007_rechnen_sie_mit_wasserstoff_v110_tcm550-169419.pdf.

[9] Water Electrolysis > Products > Home Uhde Chlorine Engineers. URL https://www.thyssenkrupp-uhde-chlorine-engineers.com/en/products/water-electrolysis-hydrogen-production.

[10] SAFETY DATA SHEET, Hydrogen, compressed, The Linde Group, URL https://produkte.linde-gas.at/sdb_konform/H2_10021694EN.pdf.

[11] S. A.G., SALCOS®, 2022, URL https://salcos.salzgitter-ag.com/en/index.html.

[12] Hydrogen: an energy carrier for the future. URL https://hydrogen.thyssenkrupp.com/en/.

[13] M. Hölling, M. Weng, S. Gellert, Bewertung der Herstellung von Eisenschwamm unter Verwendung von Wasserstoff, 2017.

[14] K. Mongird, V. Viswanathan, J. Alam, C. Vartanian, V. Sprenkle, R. Baxter, 2020 Grid energy storage technology cost and performance assessment, 2020.

[15] D. Papadias, R. Ahluwalia, Bulk storage of hydrogen, Int. J. Hydrog. Energy 46 (70) (2021) 34527–34541, http://dx.doi.org/10.1016/j.ijhydene.2021.08.028, URL https://linkinghub.elsevier.com/retrieve/pii/S0360319921030834.

[16] G. Cerbe, M. Dehli, J.E. Kätelhön, T. Kleiber, J. Kuck, B. Lendt, J. Mischner, B. Mundus, H. Pietsch, D. Spohn, W. Thielen, Grundlagen der Gastechnik, 7. vollständig neu bearbeitete Auflage, Carl Hanser Verlag München Wien, 2008, URL https://www.hanser-kundencenter.de/fachbuch/artikel/9783446449657.

[17] O.G.E. GmbH, NEP-Gas-Datenbank, FNB Gas e.V. URL https://www.nep-gas-datenbank.de:8080/app/#!/.

[18] QGIS Development Team, QGIS Software, Open Source Geospatial Foundation, 2009, URL https://www.qgis.org/en/site/.

[19] C. Wentzler, Konzeptionierung und Implementierung eines Wasserstoff-Netzwerk-Modell-Frameworks (Masterarbeit), Forschungszentrum Jülich Institut für Energie- und Klimaforschung: Techno-ökonomische Systemanalyse (IEK-3)/RWTH Aachen University, Fakultät für Maschinenwesen, 2022.

[20] M.V. Lurie, Subject Index, in: Modeling of Oil Product and Gas Pipeline Transportation, John Wiley & Sons, Ltd, 2008, pp. 207–214, http://dx.doi.org/10.1002/9783527626199.indsub, URL https://onlinelibrary.wiley.com/doi/abs/10.1002/9783527626199.indsub _eprint: https://onlinelibrary.wiley.com/doi/pdf/10.1002/9783527626199.indsub.

[21] T. Koch, B. Hiller, M.E. Pfetsch, L. Schewe, Evaluating Gas Network Capacities, in: Series on Optimization, MOS-SIAM, 2015.

[22] P. Domschke, B. Hiller, J. Lang, V. Mehrmann, R. Morandin, C. Tischendorf, Gas Network Modeling: An Overview (Extended English Version) 53.

[23] R.J. LeVeque, Finite Volume Methods for Hyperbolic Problems, in: Cambridge Texts in Applied Mathematics, Cambridge University Press, Cambridge, 2002, http://dx.doi.org/10.1017/CBO9780511791253, URL https://www.cambridge.org/core/books/finite-volume-methods-for-hyperbolic-problems/97D5D1ACB1926DA1D4D52EAD6909E2B9.

[24] D. Rose, M. Schmidt, M.C. Steinbach, B.M. Willert, Computational optimization of gas compressor stations: MINLP models versus continuous reformulations, Math. Methods Oper. Res. 83 (3) (2016) 409–444, http://dx.doi.org/10.1007/s00186-016-0533-5, URL http://link.springer.com/10.1007/s00186-016-0533-5.

[25] D. Serre, Systems of Conservation Laws 1: Hyperbolicity, Entropies, Shock Waves: Volume Undefined: Hyperbolicity, Entropies, Shock Waves, Cambridge University Press, Cambridge, 1999, http://dx.doi.org/10.1017/CBO9780511612374, URL https://www.cambridge.org/core/books/systems-of-conservation-laws-1/3E00C5069ED34D5ABBE72626A44EAB2A.

[26] A.J. Osiadacz, M.g. Kwestarz, Nonlinear Steady-State Optimization of Large-Scale Gas Transmission Networks, Energies 14 (10) (2021) 2832, http://dx.doi.org/10.3390/en14102832, URL https://www.mdpi.com/1996-1073/14/10/2832.

[27] M.E. Pfetsch, A. Fügenschuh, B. Geißler, N. Geißler, R. Gollmer, B. Hiller, J. Humpola, T. Koch, T. Lehmann, A. Martin, A. Morsi, J. Rövekamp, L. Schewe, M. Schmidt, R. Schultz, R. Schwarz, J. Schweiger, C. Stangl, M.C. Steinbach, S. Vigerske, B.M. Willert, Validation of nominations in gas network optimization: models, methods, and solutions, Optim. Methods Softw. 30 (1) (2015) 15–53, http://dx.doi.org/10.1080/10556788.2014.888426, URL http://www.tandfonline.com/doi/abs/10.1080/10556788.2014.888426.

[28] M. Gugat, R. Schultz, D. Wintergerst, Networks of pipelines for gas with nonconstant compressibility factor: stationary states, Comput. Appl. Math. 37 (2) (2018) 1066–1097, http://dx.doi.org/10.1007/s40314-016-0383-z, URL http://link.springer.com/10.1007/s40314-016-0383-z.

[29] A. Bermúdez, J. González-Díaz, F.J. González-Diéguez, Á.M. González-Rueda, M.P.F.d. Córdoba, Simulation and optimization models of steady-state gas transmission networks, Energy Procedia 64 (2015) 130–139, http://dx.doi.org/10.1016/j.egypro.2015.01.016, URL https://linkinghub.elsevier.com/retrieve/pii/S187661021500017X.

[30] Á.M. González Rueda, J. González Díaz, M. P. Fernández de Córdoba, A twist on SLP algorithms for NLP and MINLP problems: an application to gas transmission networks, Optim. Eng. 20 (2) (2019) 349–395, http://dx.doi.org/10.1007/s11081-018-9407-4, URL http://link.springer.com/10.1007/s11081-018-9407-4.

[31] B. Geißler, Towards Globally Optimal Solutions for MINLPs by Discretization Techniques with Applications in Gas Network Optimization, first ed., Verlag Dr. Hut, München, 2011.

[32] GANESO | Reganosa URL https://www.reganosa.com/en/ganeso.

[33] A. van der Schaft, Port-Hamiltonian systems: an introductory survey, in: M. Sanz-Solé, J. Soria, J.L. Varona, J. Verdera (Eds.), Proceedings of the International Congress of Mathematicians, Madrid, August 22–30, 2006, European Mathematical Society Publishing House, Zuerich, Switzerland, 2007, pp. 1339–1365, http://dx.doi.org/10.4171/022-3/65, URL http://www.ems-ph.org/doi/10.4171/022-3/65.

[34] B. Geißler, A. Morsi, L. Schewe, M. Schmidt, Solving highly detailed gas transport MINLPs: Block separability and penalty alternating direction methods, INFORMS J. Comput. 30 (2) (2018) 309–323, http://dx.doi.org/10.1287/ijoc.2017.0780, URL http://pubsonline.informs.org/doi/10.1287/ijoc.2017.0780.

[35] B. Geißler, A. Morsi, L. Schewe, M. Schmidt, Solving power-constrained gas transportation problems using an MIP-based alternating direction method, Comput. Chem. Eng. 82 (2015) 303–317, http://dx.doi.org/10.1016/j.compchemeng.2015.07.005, URL https://linkinghub.elsevier.com/retrieve/pii/S0098135415002409.

[36] A. Fugenschuh, B. Hiller, J. Humpola, T. Koch, T. Lehmann, R. Schwarz, J. Schweiger, J. Szabo, Gas network topology optimization for upcoming market requirements, in: 2011 8th International Conference on the European Energy Market, EEM, IEEE, Zagreb, Croatia, 2011, pp. 346–351, http://dx.doi.org/10.1109/EEM.2011.5953035, URL http://ieeexplore.ieee.org/document/5953035/.

[37] W.E. Hart, J.-P. Watson, D.L. Woodruff, Pyomo: modeling and solving mathematical programs in Python, Math. Program. Comput. 3 (3) (2011) 219–260.

[38] W.E. Hart, C. Laird, J.-P. Watson, D.L. Woodruff, G.A. Hackebeil, B.L. Nicholson, J.D. Siirola, Pyomo – Optimization Modeling in Python, Springer, 2017.

[39] I.H. Bell, J. Wronski, S. Quoilin, V. Lemort, Pure and pseudo-pure fluid property evaluation and the open-source thermophysical property library CoolProp, Ind. Eng. Chem. Res. 53 (6) (2014) 2498–2508, http://dx.doi.org/10.1021/ie4033999, URL http://pubs.acs.org/doi/abs/10.1021/ie4033999.

[40] Gurobi Optimizer Reference Manual, Gurobi Optimization, LLC, URL https://www.gurobi.com/wp-content/plugins/hd_documentations/documentation/9.0/refman.pdf.

[41] J. Nikuradse, Laws of Flow in Rough Pipes, 1950, URL https://ntrs.nasa.gov/citations/19930093938 NTRS Author Affiliations: NTRS Report/Patent Number: NACA-TM-1292 NTRS Document ID: 19930093938 NTRS Research Center: Legacy CDMS (CDMS).

[42] Energiepark Bad Lauchstädt URL https://energiepark-bad-lauchstaedt.de/.

[43] Wasserstoffprojekt am Standort Hamburg-Moorburg Vattenfall, URL https://group.vattenfall.com/de/newsroom/pressemitteilungen/2021/wasserstoffprojekt-am-standort-hamburg-moorburg.

[44] swb A.G., Elektrolyseur am Stahlwerk | Wasserstoff | swb, URL https://www.swb.de/ueber-swb/unternehmen/nachhaltigkeit/wasserstoff/elektrolyseur,

[45] Implementation – GET H2 – Mit Wasserstoff bringen wir gemeinsam die Energiewende voran, URL https://www.get-h2.de/en/implementation/.

[46] Lingen Green Hydrogen – decarbonising the industry with sustainable fuel, Lingen Green Hydrogen, URL https://lingen-green-hydrogen.com/en/.

[47] Grüner Wasserstoff für grünen Stahl aus Duisburg, STEAG GmbH URL https://www.steag.com/de/pressemitteilung/03-12-2020-gruener-wasserstoff-fuer-gruenen-stahl-aus-duisburg.

[48] GET H2 Nukleus, OGE URL https://oge.net/en/us/projects/our-hydrogen-projects/get-h2-nukleus.

[49] IndustriePark Lingen - Aktuelles URL https://www.industriepark-lingen.de/aktuelles/aktuelles.html.

[50] Westwind Energy erklärt Hintergründe für geplanten Windpark im Brockumer Fladder https://www.kreiszeitung.de URL https://www.kreiszeitung.de/lokales/diepholz/lemfoerde-ort48657/westwind-windpark-windenergieanlagen-windkraft-brockum-duemmer-90122432.html Section: Lokales.

[51] Die Entstehung einer grünen Wasserstoffwirtschaft Storengy URL https://www.storengy.de/de/medien/nachrichten/die-entstehung-einer-gruenen-wasserstoffwirtschaft.